Modified technique for processing multiangle lidar data measured in clear and moderately polluted atmospheres

Vladimir Kovalev,* Cyle Wold, Alexander Petkov, and Wei Min Hao

Forest Service, U.S. Department of Agriculture, Fire Sciences Laboratory, 5775 Highway 10 West, Missoula, Montana 59808, USA

*Corresponding author: vkovalev@fs.fed.us

Received 7 April 2011; revised 17 June 2011; accepted 26 July 2011; posted 27 July 2011 (Doc. ID 145456); published 0 MONTH 0000

We present a modified technique for processing multiangle lidar data that is applicable for relatively clear atmospheres, where the utilization of the conventional Kano–Hamilton method meets significant issues. Our retrieval algorithm allows computing the two-way transmission and the corresponding extinction-coefficient profile in any slope direction searched during scanning. These parameters are obtained from the backscatter term of the Kano–Hamilton solution and the corresponding square-range-corrected signal; the second component of the solution, related with the vertical optical depth, is completely excluded from consideration. The inversion technique was used to process experimental data obtained with the Missoula Fire Sciences Laboratory lidar. Simulated and real experimental data are presented that illustrate the essentials of the data-processing technique and possible variants of the extinction-coefficient profile retrieval.

OCIS codes: 280.3640, 290.1350, 290.2200.

1. Introduction

The classical Kano–Hamilton multiangle method allows the extraction of the particulate extinction coefficient from elastic lidar data without an *a priori* assumption on the vertical profile of the lidar ratio and without the need to determine the lidar solution constant through the assumption of the aerosol-free atmosphere. However, the method works only in horizontally stratified atmospheres and requires fulfilling two conditions [1,2]. First, within the lidar operative zone, the total backscatter coefficient along the horizontal direction at any height h should be invariable, that is,

$$\beta_\pi(h) = \text{const.} \tag{1}$$

In practice, this requirement means that the vertical profile $\beta_\pi(h)$ should be the same for any slope direction used for the scanning. The second condition is the rigorous dependence of the slope optical depth $\tau_i(0,h)$, measured along the elevation angle φ_i, on this angle. The dependence is

$$\tau_i(0,h) = \frac{\tau_{90}(0,h)}{\sin\varphi_i}. \tag{2}$$

Here $\tau_{90}(0,h)$ is the total optical depth of the layer from ground level ($h=0$) to h in the vertical direction. The same as $\tau_{90}(0,h)$, the slope optical depth $\tau_i(0,h)$ includes both the aerosol and the molecular components, so that $\tau_i(0,h) = \tau_{m,i}(0,h) + \tau_{p,i}(0,h)$. Similarly, the backscatter coefficient $\beta_\pi(h) = \beta_{\pi,m}(h) + \beta_{\pi,p}(h)$ is the sum of the molecular and particulate components of the backscatter coefficient.

In the classic Kano–Hamilton method, the set of the functions $y_i(h)$ are calculated from the lidar signals $P_i(h)$ measured under different elevation angles φ_i. These functions are defined as

0003-6935/11/240001-01$15.00/0

$$y_i(h) = \ln[P_i(h)(h/\sin\varphi_i)^2]. \tag{3}$$

The term in the rectangular brackets is the square-range-corrected signal at the height h, measured along the elevation angle φ_i relative to the horizon. If the assumptions in Eqs. (1) and (2) are valid, the function $y_i(h)$ can be rewritten in the form

$$y_i(h) = A(h) - \frac{2\tau_{90}(0,h)}{\sin\varphi_i}, \tag{4}$$

where

$$A(h) = \ln[C\beta_\pi(h)], \tag{5}$$

and C is the lidar solution constant, which includes the laser emitting power, whose variations, if such occur during the scanning, should be compensated.

In the atmosphere in which Eqs. (1) and (2) are satisfied, the slope of the linear fit of the functions $y_i(h)$ versus the independent $x_i = [\sin\varphi_i]^{-1}$ is proportional to the optical depth $\tau_{90}(0,h)$, from which the basic function of interest, the extinction coefficient, can then be extracted. The intersect of the linear fit of $y_i(h)$ with the y axis, obtained through extrapolation of the fit, determines the function $A(h)$ in Eq. (5), that is, it shows the relative behavior of the backscatter coefficient profile with height. Until recently, this function was not the subject of researchers' interest; they focused mainly on determining the slope of the linear fit to then obtain the optical depth and the extinction coefficient.

The first common issue met by a researcher is the retrieval of accurate profiles of the optical depth. In real atmospheres, the requirements in Eqs. (1) and (2) are satisfied, at best, only approximately, so that the profiles of $\tau_{90}(0,h)$ retrieved from the multiangle data are often distorted. The relative error in the retrieved $\tau_{90}(0,h)$ can be unacceptably large, especially in clear atmospheres, where the difference in the optical depths measured under adjacent elevation angles is small and the relative error of the derived particulate extinction coefficient can range from tens to even hundreds of percent [3]. Various methods have been proposed to reduce this large uncertainty when numerical differentiation is used to determine the slope of the linear fit [4–8]; however, the problem cannot be considered as being satisfactorily solved.

Another deficiency of the classical Kano–Hamilton solution is the extremely poor inversion efficiency. To obtain a single vertical optical depth profile $\tau_{90}(0,h)$, one should measure and then process at least a dozen lidar signals measured in different elevation angles. There is no simple and practical method to select the good data and exclude the signals from the slope directions where the requirements in Eqs. (1) and (2) are not satisfied. Moreover, to the best of our knowledge, no reliable method exists that takes into consideration the distortions in the retrieved optical depth due to systematic distortions in the recorded signal. Meanwhile, the uncertainty estimates based on purely statistical methods can yield underestimated measurement errors.

The goal of the current study is to develop the data-processing methodology that would allow us (a) to check the validity of Eqs. (1) and (2) in the multiangle measurements and determine the heights where these requirements are not properly met, (b) to analyze individually the transmission profiles in different slope directions in order to locate and exclude the data under the elevation angles where the presence of local layering violates the condition of the atmospheric horizontal homogeneity, and (c) to exclude the large uncertainty related with the numerical differentiation of the noisy optical depth function.

To achieve these goals, we developed an alternative data-processing methodology. In this technique, the individual lidar signals can be independently inverted into the required optical parameters. This approach allows the determination of the extinction-coefficient profiles at different elevation angles and compares these to each other. Such a comparison provides better understanding of the real uncertainties of the retrieved optical properties in the searched atmosphere due to the violation of the requirements in Eqs. (1) and (2). The key specific of the modified technique is that the slope component in Eq. (4), related with $\tau_{90}(0,h)$, is completely excluded from consideration. Instead, the two-way transmittance in any selected slope direction φ_i is obtained from the exponent of the function $A(h)$ in Eq. (5) and the corresponding square-range-corrected signal $P_i(h)(h/\sin\varphi_i)^2$.

2. Method

A. Substantiation of the Modified Multiangle Data-Processing Technique for the Lidar Data Measured in Clear and Moderately Polluted Atmospheres

In clear atmosphere, the use of the slope method to determine backscatter from the intercept yields better accuracy than the retrieval of extinction from the slope [9]. Recently, a number of investigations have been made in which the authors analyzed extracting the extinction coefficient by using the information contained in the backscatter term [10–14]. In this study, we consider the variant of a multiangle solution in which the most challenging operations of determining $\tau_{90}(0,h)$ from Eq. (4) and the extinction coefficient from $\tau_{90}(0,h)$ are omitted. The Kano–Hamilton solution is reduced to determining the function $[C\beta_\pi(h)]$ by calculating the exponent of $A(h)$. This exponential function and the profile of the range-corrected signal, measured in a selected slope direction (or directions), are the functions from which the basic function of interest, the extinction coefficient of the searched atmosphere, is obtained.

Before discussing the details of this technique, let us consider how the violation of the requirements in Eqs. (1) and (2) influences the accuracy of the retrieved $[C\beta_\pi(h)]$. To obtain such estimates, numerical experiments were performed. As only systematic distortions are the subject of our interest, the simple two-point multiangle solution was utilized. Particularly, in our calculations, we considered an artificial lidar that operates at the wavelength 355 nm along two elevation angles, $\varphi_1 = 90°$ and $\varphi_2 = 30°$. Initially we analyzed the case when, at the height of interest, $h = 1000$ m, the requirement in Eq. (1) was poorly met, that is, $\beta_{\pi,30}(h) \neq \beta_{\pi,90}(h)$. We assumed that the backscatter coefficient in the slope direction φ_2 may differ by $\pm 30\%$ relative to that in the vertical direction φ_1. In such a case, instead of the true fit $y(h)$, when $\beta_{\pi,30}(h) = \beta_{\pi,90}(h)$, the linear fits give two distorted lines, $y'(h)$ and $y''(h)$, corresponding to the negative and positive shift in $\beta_{\pi,30}(h)$, respectively (Fig. 1). The calculations show that the corresponding distortions in the vertical optical depth $\tau_{90}(0,h)$ and in our function of interest, $[C\beta_\pi(h)]$, which is found as the exponent of $A(h)$, will be different. The difference depends on the total optical depth $\tau_{90}(0,h)$ of the layer from ground level to the selected height. In Fig. 2, the relative errors in the total and particulate optical depths versus $\tau_{90}(0,h)$ (the dotted and dashed curves, respectively) are shown for two cases, $\beta_{\pi,30}(h) = 0.7\beta_{\pi,90}(h)$ and $\beta_{\pi,30}(h) = 1.3\beta_{\pi,90}(h)$. The thick solid curves show the corresponding relative errors in $[C\beta_\pi(h)]$. One can see that, in such air conditions, the relative error in $[C\beta_\pi(h)]$ is smaller than the error in the retrieved optical depth up to $\tau_{90}(0,h) \leq 0.45$. One should also keep in mind that the errors in the function $[C\beta_\pi(h)]$ are much less influential because, unlike the optical depth, this function is not differentiated in order to obtain the extinction coefficient.

We have analyzed also how the error in the retrieved $[C\beta_\pi(h)]$ depends on the violation of the requirement in Eq. (2). Similar to the previous case, the linear fit $y(h)$ corresponds to the atmosphere where the requirement in Eq. (2) is met, that is, the slope of this function yields the true optical depth $\tau_{90}(0,h)$. The linear fit $y'(h)$ is obtained in an atmosphere where the above requirement is not valid, so that its slope yields the erroneous value $\tau'_{90}(0,h)$. The Kano–Hamilton solutions for these two cases may be written as $y(h) = \ln[C\beta_\pi(h)] - [2\tau_{90}(0,h)]x$ and $y'(h) = \ln[C\beta'_\pi(h)] - [2\tau'_{90}(0,h)]x$, respectively; here, $[C\beta'_\pi(h)]$ is the erroneous intercept that corresponds to the erroneous $y'(h)$ (Fig. 1). In the intersection point $x = x_0$, $y(h) = y'(h)$ and, accordingly,

$$\ln\left[\frac{\beta'_\pi(h)}{\beta_\pi(h)}\right] = -2x_0[\tau_{90}(0,h) - \tau'_{90}(0,h)]. \tag{6}$$

Defining the difference between $\tau'_{90}(0,h)$ and $\tau_{90}(0,h)$ as $\Delta\tau_{90}(0,h)$, and the corresponding relative error in the backscatter coefficient as $\delta = \beta'_\pi(h)/\beta_\pi(h) - 1$, one can obtain the relative error δ as

$$\delta = \exp[2x_0\Delta\tau_{90}(0,h)] - 1. \tag{7}$$

As follows from Eq. (7), the relative error δ depends on the difference between the optical depths in the directions φ_1 and φ_2 and the location of the interception point x_0, and does not depend on the optical depth $\tau_{90}(0,h)$. In Fig. 2, the error calculated for $x_0 = 1$ and $\Delta\tau_{90}(0,h) = \pm 0.05$ is shown as two solid horizontal lines with filled circles. If the intersection of the above linear fits occurs at $x_0 = 2$, the errors δ become larger, −18% and 22%; they still remain less than the error in the total optical depth up to $\tau_{90}(0,h) \sim 0.6$. In some cases, the uncertainty can be reduced by shifting the intersection point x_0 to the point $x_{\min}$, which corresponds to the elevation angle $\varphi_{\max}$. In this case, the intersection $A(h)$ is shifted to $A'(h) = y(h, x_{\min}) + 2\tau'_{90}(0,h)x_{\min}$.

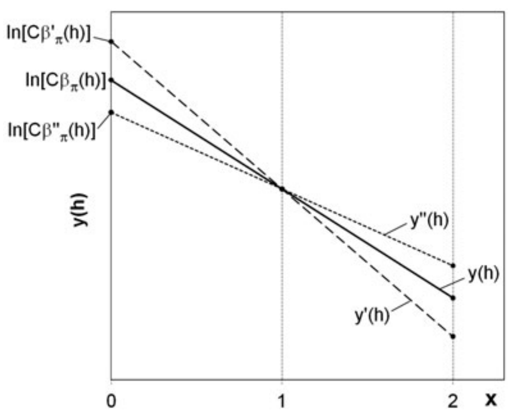

Fig. 1. True linear fit $y(h)$ (solid line), and two shifted lines, $y'(h)$ and $y''(h)$, obtained due to the violation of the requirement of a horizontally stratified atmosphere in Eq. (1). The dashed line, $y'(h)$, is obtained when $\beta_{\pi,30}(h) = 0.7\beta_{\pi,90}(h)$, and the dotted line, $y''(h)$, is obtained when $\beta_{\pi,30}(h) = 1.3\beta_{\pi,90}(h)$. The intersection points at $x = 0$ are obtained by extrapolating the linear fits determined for the points $x = 1$ and $x = 2$.

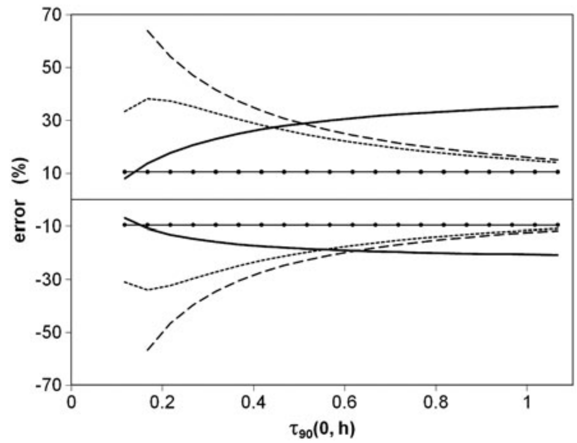

Fig. 2. Dependence of the relative errors in the total and particulate optical depths (dotted and dashed curves, respectively) and the corresponding errors in $[C\beta_\pi(h)]$ (thick solid curves) versus total vertical optical depth for the cases shown in Fig. 1. The solid horizontal lines with filled circles represent the errors in the profiles $[C\beta_\pi(h)]$, caused by the violation of the requirement of a stratified atmosphere in Eq. (2); here $x = 1$ and $\Delta\tau_{90}(0,h) = \pm 0.05$.

B. Extraction of the Slope Transmission Profile from $[C\beta_\pi(h)]$ and the Corresponding Square-Range-Corrected Signal and Determination of the Extinction Coefficient through Numerical Differentiation

The schematic of the measurement, which clarifies the data-processing technique, is shown in the right panel of Fig. 3. The slope lines in the right panel show the directions of lidar scanning. The direction shown as a thick line clarifies the signs used in the formulas. To avoid superfluous details in the figure, only some elevation angles are shown. The solid and dashed spherical arcs show the minimum and maximum measurement ranges of the lidar, $r_{\min}$ and $r_{\max}$, so that the lidar signals are recorded within the heights from $h_{i,\min} = r_{\min} \sin \varphi_i$ to $h_{i,\max} = r_{\max} \sin \varphi_i$, respectively. For simplicity, we assume that $r_{\min}$ and $r_{\max}$ are the same for all elevation angles.

Let us consider initially an artificial lidar that scans a synthetic atmosphere at the wavelength 355 nm within the slope angular sector from 10° to 90° and its measurement range extends from $r_{\min} = 500\,\mathrm{m}$ to $r_{\max} = 7000\,\mathrm{m}$. The particulate extinction coefficient in the synthetic atmosphere decreases with height, from $\kappa_p(h) = 0.15\,\mathrm{km}^{-1}$ at ground level to $\kappa_p(h) = 0.011\,\mathrm{km}^{-1}$ at $h = 7000\,\mathrm{m}$. In addition, two horizontally stratified turbid layers exist with $\kappa_p(h) = 0.25\,\mathrm{km}^{-1}$ at the altitudes from 2500 to 3000 m and with $\kappa_p(h) = 0.1\,\mathrm{km}^{-1}$ at the altitudes from 3500 to 3800 m. The model lidar ratio is variable; from ground level to the height 1000 m, it is 20 sr, within both turbid layers it is 60 sr, and outside these layers it is 30 sr. The $[C\beta_\pi(h)]$ profile, determined with the Kano–Hamilton method within the altitude range from $h_{\min} = 180\,\mathrm{m}$ to $h_{\max} = 5000\,\mathrm{m}$ is shown in Fig. 3 on the left side. Note that the maximal height $h_{\max}$, where the profile $[C\beta_\pi(h)]$ can be found from the Kano–Hamilton solution, is always less than the maximal lidar range $r_{\max}$. Accordingly, under large elevation angles, the maximal range is reduced to meet the requirement $h_{i,\max} \le h_{\max}$.

The square-range-corrected signal in the slope direction φ_i versus range r_i can be written as

$$P_i(r_i) r_i^2 = C\beta_\pi(r_i) T^2_{\mathrm{tot},i}(0, r_i), \qquad (8)$$

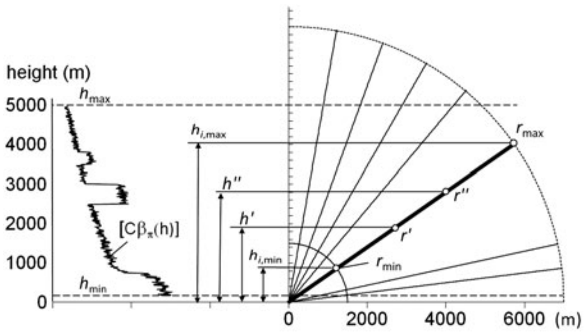

Fig. 3. Schematic of the multiangle measurement (right panel) and the vertical profile of $[C\beta_\pi(h)]$ extracted from the whole set of multiangle data (left panel).

where $T^2_{\mathrm{tot},i}(0, r_i)$ is the total two-way transmittance along the slope direction φ_i, from the starting point $r = 0$ to r_i, which varies within the range $r_{\min} \le r_i \le r_{\max}$. This function is the product of the particulate and molecular components $T^2_{p,i}(0, r_i)$ and $T^2_{m,i}(0, r_i)$, respectively. Using the signal in Eq. (8) and the function $[C\beta_\pi(h)]$ derived from the Kano–Hamilton solution, one can extract the corresponding profile $T^2_{\mathrm{tot},i}(0, r_i)$ within the height interval from $h_{i,\min}$ to $h_{i,\max}$ with the formula

$$T^2_{\mathrm{tot},i}(0, r_i) = \frac{P_i(r_i) r_i^2}{[C\beta_\pi(h_i)]}, \qquad (9)$$

where $h_i = r_i \sin \varphi_i$.

Two-way particulate transmittance $T^2_{p,i}(0, r_i)$ can be determined as the ratio of $T^2_{\mathrm{tot},i}(0, r_i)$ and the known molecular profile $T^2_{m,i}(0, r_i)$. The corresponding particulate extinction coefficient along the slope direction φ_i can be found using different methods. The most straightforward way is the determination of the extinction coefficient by calculating the sliding derivative of the logarithm of the two-way particulate transmittance $T^2_{p,i}(0, r_i)$, i.e.,

$$\kappa_p^*(r_i) = -0.5 \frac{d}{dr} \ln[T^2_{p,i}(0, r_i)]. \qquad (10)$$

Note that, when the slope directions are analyzed, the increments of the slope range r, rather than the height, are used in the differentiation procedure. In this case, generally more accurate extinction-coefficient profiles are obtained as compared with the conventional way of extracting $\kappa_p(h)$ from $\tau_{90}(0, h)$. This can be achieved only if the level of noise fluctuation in $T^2_{p,i}(0, r_i)$ is relatively low.

An example of a two-way particulate transmittance profile extracted from the profile $[C\beta_\pi(h)]$ and the signal measured at $\varphi_i = 90°$ is shown in Fig. 4 as the thin dashed curve; the thick solid curve is the actual model profile for the synthetic atmosphere under consideration. Our simulated data are corrupted

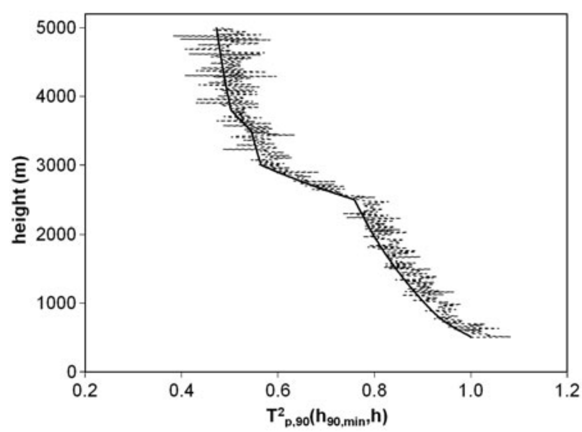

Fig. 4. Model profile of the vertical two-way particulate transmittance $T^2_{p,90}(h_{90,\min}, h)$ (solid curve) and that extracted from the lidar multiangle data (dashed curve).

with quasi-random noise and, accordingly, the retrieved profile $T^2_{p,90}(h_{90,\min}, h)$ is slightly shifted relative to the model profile. The particulate extinction coefficient versus height $\kappa^*_p(h)$ extracted with the numerical differentiation from $T^2_{p,90}(h_{90,\min}, h)$ is shown in Fig. 5 as the thick solid curve. The curves with the filled triangles and the open circles show the vertical extinction-coefficient profiles extracted from the lidar signals measured at $\varphi_i = 30°$ and $\varphi_i = 45°$, respectively, and the thin solid curve shows the model profile of $\kappa_p(h)$ for the synthetic atmosphere used in the numerical experiment. All the profiles $\kappa^*_p(h)$ are extracted with the relatively large range resolution (1000 m); the smaller resolution yields extremely noisy profiles of $\kappa^*_p(h)$.

The extinction-coefficient profiles shown in Fig. 5 illustrate the typical drawback of the numerical differentiation: over distant ranges, the presence of random noise does not allow one to discriminate thin aerosol layers. Neither the use of the signal at $\varphi_i = 90°$ nor its use that at $\varphi_i = 45°$ allows discrimination of the second layer at heights of 3500–3800 m. The profile of $\kappa^*_p(h)$ extracted from the signal at $\varphi_i = 45°$ shows some increase in the aerosol loading at high altitudes; however, the location of the retrieved aerosol loading at heights of 3400–4500 m is wrong. Unfortunately, the determination of the sharp perturbations in the atmosphere is always an issue, especially when the differentiating technique is used for distant ranges [15,16].

Thus, because of the square-range-corrected signal measured by lidar is always noisy, especially over distant ranges, the corresponding profile of $T^2_{p,i}(r_{\min}, r_i)$ has randomly distributed bulges and concavities. Accordingly, its numerical differentiation yields extremely noisy profiles of $\kappa^*_p(r_i)$ over distant ranges. As shown in the next section, the use of the backscattering term $[C\beta_\pi(h)]$, in which the perturbations are well defined, allows extracting the much more accurate extinction-coefficient profile over distant ranges.

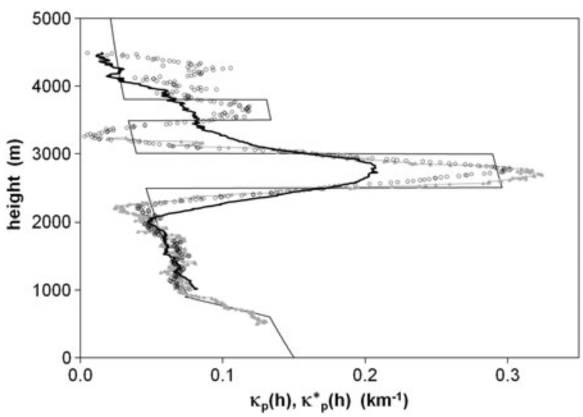

Fig. 5. Profiles of $\kappa^*_p(h)$ obtained by the numerical differentiation of the profiles $T^2_{p,i}(h_{i,\min}, h)$ retrieved from the lidar signals measured at $\varphi_i = 90°$ (thick solid curve), $\varphi_i = 30°$ (gray curve with filled triangles), and $\varphi_i = 45°$ (open circles). The thin solid curve is the model profile of the synthetic atmosphere used for the simulations.

C. Extraction of the Extinction-Coefficient Profile by Equalizing Two Alternative Transmittance Profiles

In this section, we will consider an alternative variant of the extraction of the extinction coefficient from the slope transmission profile obtained with Eq. (9), using the assumption of a range-independent column lidar ratio over restricted slope range intervals. To apply such a variant, the total range of the lidar signal from $r_{\min}$ to $r_{\max}$, measured in the selected slope or vertical direction, should be divided into a number of smaller intervals, (r', r''). For each such interval, the profile of the particulate transmittance is determined using the corresponding pieces of the profile $T^2_{\mathrm{tot},i}(0, r_i)$ [Eq. (9)] and the molecular profile $T^2_{m,i}(0, r_i)$. The particulate transmission profile along the slope direction φ_i within the restricted interva $r' \le r_i \le r''$ is found as

$$T^2_{p,i}(r', r_i) = \frac{T^2_{\mathrm{tot},i}(0, r_i) T^2_{m,i}(0, r')}{T^2_{\mathrm{tot},i}(0, r') T^2_{m,i}(0, r_i)}. \qquad (11)$$

Now for this interval, (r', r''), the alternative two-way transmission $\langle T^2_{p,i}(r', r_i)\rangle$ that best matches $T^2_{p,i}(r', r_i)$ should be found. This can be done by using the assumption of the range-independent column-integrated lidar ratio within the interval (r', r''). The above transmission profiles, $T^2_{p,i}(r', r_i)$ and $\langle T^2_{p,i}(r', r_i)\rangle$, are equalized by selecting an appropriate value of the column lidar ratio for the second profile. To trigger this procedure, a particulate column-integrated lidar ratio $S_{p,i}(r', r_i)$, invariable within the interval (r', r''), is arbitrarily selected. The corresponding profile of the particulate extinction coefficient within the corresponding height interval from $h' = r' \sin\varphi_i$ to $h'' = r'' \sin\varphi_i$ is calculated as

$$\kappa_p(h) = S_{p,i}(h', h)\beta_{\pi,p}(h), \qquad (12)$$

where $\beta_{\pi,p}(h)$ is the profile of the particulate backscatter coefficient extracted from the profile $[C\beta_\pi(h)]$ (the method of this extraction is discussed below). The corresponding two-way transmittance within the range from r' to r'' is found as

$$\langle T^2_{p,i}(r', r_i)\rangle = \exp\left[-2\int_{r'}^{r_i} \kappa_p(x)\mathrm{d}x\right]. \qquad (13)$$

The profile obtained with Eq. (13) is compared with that obtained in Eq. (11). As the primary column-integrated lidar ratio $S_{p,i}(r', r_i) = \mathrm{const.}$ is selected arbitrarily, the profiles $T^2_{p,i}(r', r_i)$ and $\langle T^2_{p,i}(r', r_i)\rangle$ within the range (r', r'') initially generally diverge. These transmission profiles can be equalized by selecting the appropriate column-integrated lidar ratio in Eq. (12). To determine how close the profiles $T^2_{p,i}(r', r_i)$ and $\langle T^2_{p,i}(r', r_i)\rangle$ are, a simple criterion is implemented that compares the slopes of the linear fits of these profiles over the selected range (r', r''). As both profiles decrease with range, the linear fits of these can be written in the standard form

$$T_{p,i}^2(r', r_i) = A_1 - B_1 r_i, \tag{14}$$

$$\langle T_{p,i}^2(r', r_i)\rangle = A_2 - B_2 r_i. \tag{15}$$

The only task now is to find such a column-integrated lidar ratio $S_p(r', r_i)$ that minimizes the criterion

$$\Lambda = (B_1 - B_2)^2. \tag{16}$$

After the criterion Λ is minimized, the corresponding profile of $\kappa_p(h)$ in Eq. (12) is taken as the extinction-coefficient profile of interest over the corresponding altitude range from h' to h''. The operations in Eqs. (11)–(16) are repeated for all the piecewise zones (r', r'') selected within the altitude range $(h_{i,\min}, h_{i,\max})$. For each such interval, the constant column-integrated lidar ratio is found that minimizes the value of Λ in Eq. (16).

The use of the linear fit for the transmission profile $T_{p,i}^2(r', r_i)$ makes it also possible to elaborate on the maximal measurement range of the lidar signal, $r_{\max}$. There is a simple requirement, $B_1 > 0$, which should be met when selecting the last interval (r'_N, r''_N). If this inequality is not met, the two-way transmission in this interval will have an unphysical increase within this range; the only possibility to satisfy the requirement of the positive B_1 is to reduce the maximal range $r_{\max}$ as much as necessary to obtain $B_1 > 0$. Note also that the physical minimum $B_1 = 0$ means that there is no particulate component in this range interval (or it is too small to be determined from the measurement data).

The above method of determining the extinction coefficient does not require numerical differentiation. However, it requires knowledge of the particulate backscatter coefficient $\beta_{\pi,p}(h)$ in Eq. (12). Obviously, this profile can be determined from the same function $[C\beta_\pi(h)]$ if the constant C is someway estimated. In the clear atmospheres for which this method is basically assumed, the constant can be found by using the conventional assumption of pure molecular scattering at high altitudes. If a reference height h_{ref} is selected somewhere close to the maximal height, and the backscatter coefficient $\beta_{\pi,p}(h_{\text{ref}}) = 0$, then the constant C can be found as

$$C = \frac{[C\beta_\pi(h_{\text{ref}})]}{\beta_{\pi,m}(h_{\text{ref}})}. \tag{17}$$

Unlike conventional methods, the vertical lidar signal is not used here for determining C. This feature can provide a more accurate determination of the constant as compared to that found from the small lidar signal at the far-end range. As one can see in Fig. 3, $h_{\max}$ is always less than $r_{\max}$. Therefore, it is useful additionally to estimate the maximal value of C with the formula

$$C \le \min \gamma(h), \tag{18}$$

where

$$\gamma(h) = \frac{[C\beta_\pi(h)]}{\beta_{\pi,m}(h)}. \tag{19}$$

The function $\gamma(h)$ is determined within the total height interval $h_{\min} \le h \le h_{\max}$ in which $[C\beta_\pi(h)]$ is known. After C is estimated, the particulate backscatter coefficient profile required for Eq. (12) is found as

$$\beta_{\pi,p}(h) = \frac{[C\beta_\pi(h)]}{C} - \beta_{\pi,m}(h). \tag{20}$$

As follows from Eqs. (18)–(20), the selection of the constant C larger than the minimum of $\gamma(h)$ will result in the zones with negative values of $\beta_{\pi,p}(h)$ within the analyzed height interval.

Let us consider the results obtained with this method using the signals of the same artificial scanning lidar in the same synthetic atmosphere described in Subsection 2.B. As stated above, before starting the retrieval procedure, one should select the number and location of the piecewise intervals (r', r'') within which the column-integrated lidar ratio will be assumed a constant. One should also decide whether they will be equal or will increase with range, and whether they will overlap. The overlapping ranges allow using additional criteria to reduce the measurement error in the areas of sharp changes of the lidar ratio, of which the location and boundaries are not known. Increasing the intervals with range reduces the influence of the increased random noise at the distant ranges. To use such variable intervals, a factor $\varepsilon \ge 1$ is implemented. If the length of the first interval is Δr_1, the next interval $\Delta r_2 = \varepsilon \Delta r_1$, then $\Delta r_3 = \varepsilon^2 \Delta r_1$, and the last interval, $\Delta r_N = \varepsilon^{N-1} \Delta r_1$. Obviously, if the factor, $\varepsilon = 1$, then $\Delta r_1 = \Delta r_2 = \ldots = \Delta r_N$, otherwise, the intervals increase with range. In Fig. 6, the locations and the lengths of eight overlapping intervals selected for the slope range from $r_{\min} = 500$ m to $r_{\max} = 7000$ m are shown. Here $\Delta r_1 = 1000$ m and $\varepsilon = 1.1$. The first range interval starts at $r'_1 = r_{\min}$ and ends at $r''_1 = r_{\min} + \Delta r_1$; the second starts at $r'_2 = r_{\min} + m\Delta r_1$, where $m < 1$ (in our calculations, the overlapping factor $m = 0.5$)

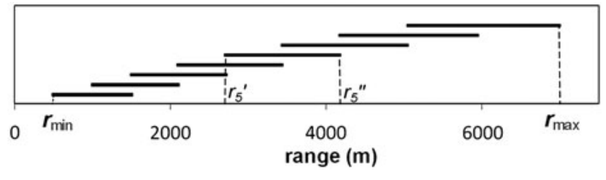

Fig. 6. Schematic of the eight overlapping intervals selected for the total measurement range from $r_{\min} = 500$ m to $r_{\max} = 7000$ m. To clarify the symbols used in the text, the beginning and the end of the fifth interval, the ranges r'_5 and r''_5, are marked.

and ends at $r''_2 = r'_2 + \Delta r_2$. The third interval starts at $r'_3 = r''_1$ and ends at $r''_3 = r'_3 + \Delta r_3$; the fourth interval starts at $r'_4 = r''_2$ and ends at $r''_4 = r'_4 + \Delta r_4$, and so on. The last interval starts at $r'_8 = r''_6$ and ends at $r''_8 = r_{\max}$. In order not to complicate Fig. 6, only the ranges r'_5 and r''_5 are marked.

In Fig. 7, the resulting, that is, "sewed together" piecewise profile of the extinction coefficient $\kappa_p(h)$ is shown as a thick black curve. The profile is obtained after minimizing Λ for each piecewise zone and averaging two overlapping extinction-coefficient profiles. For the retrieval, the maximal constant was used, determined from Eq. (18) as $C_{\max} = \min \gamma(h)$. The constant proved to be as much as 8% higher than the model value C taken for the numerical experiments. The increased value was obtained because the condition of the purely molecular scattering at the reference altitude (5000 m) was not met. Unlike the profiles obtained with the numerical differentiation (Fig. 5), where even the position of the thin far-end layers can hardly be determined, here both layers at the far range can be easily distinguished. However, this observation is not true when the constant C is significantly underestimated. The gray filled dots in the figure show the inversion result obtained from the same data, but when the constant is 2 times less than the actual C. In the areas showing slight variations of the aerosol loading and the invariable lidar ratio, such an underestimated C does not distort the retrieved profile of the extinction coefficient significantly. However, in the vicinity of sharp changes of the extinction coefficient and the lidar ratio, the underestimated C yields significant distortions in the retrieved $\kappa_p(h)$.

At the lower heights, more accurate extinction-coefficient profiles can be obtained by using the signals measured under smaller elevation angles. This effect is because the sharp changes in the vertical lidar ratio are generally reduced along low angles when they are recalculated in the slope direction with the same range resolution. In Fig. 8, the inversion results are shown for the same case as above, but where the transmittance profiles were extracted from the signal measured under the slope direction $\varphi_i = 45°$. The same as before, the thick solid curve is the retrieved extinction coefficient $\kappa_p(h)$ and the thin solid curve is the model profile of $\kappa_p(h)$. The dashed line shows the profile of $\kappa^*_p(h)$ obtained through numerical differentiation with the range resolution of 510 m. In principle, such a decreased range resolution relative to that used before (1000 m) makes it possible to discriminate both heterogeneous layers. However, the intense noise spikes mask the second layer, and it is impossible to establish which spike is originated in the increased aerosol loading and which is originated in the noise.

Let us summarize the main points of the retrieval technique. The basic idea of the method is the same as in the studies [13,14], that is, to extract the piecewise extinction coefficient from the function $[C\beta_\pi(h)]$ rather than from the optical depth. Two alternative profiles of the two-way transmittance are determined and equalized. The first one is extracted using the function $[C\beta_\pi(h)]$ and the range-corrected signal in a selected slope (or vertical) direction, φ_i; the second is retrieved directly from the function $[C\beta_\pi(h)]$ using the assumption that the piecewise column-integrated lidar ratios are invariable within restricted range intervals (r', r'') within the total measurement range $(r_{\min}, r_{\max})$.

3. Experimental Results

To demonstrate how the method works in a real atmosphere, let us consider some experimental data obtained with scanning lidar in moderately clear atmospheres. The lidar measurements were made using a mobile Q-switched Nd:YAG scanning elastic lidar with the scan ranges 0°–180° in azimuth and 0°–90° in elevation. To collect the backscattered

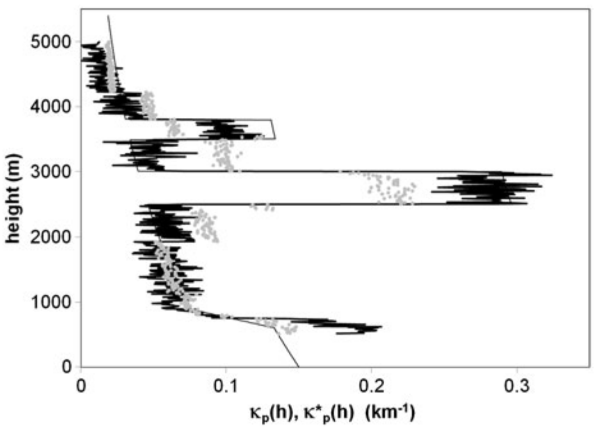

Fig. 7. Profiles of the particulate extinction coefficient $\kappa_{p,90}(h)$ extracted from $T^2_{p,90}(h_{90,\min}, h)$ presented in Fig. 4. The thick black curve shows $\kappa_p(h)$ extracted using the constant $C_{\max} = 1.08C$, whereas the gray dots show the extinction coefficient retrieved with the constant C that is 2 times less than the model value. The thin solid curve is the model profile of the extinction coefficient, the same as in Fig. 5.

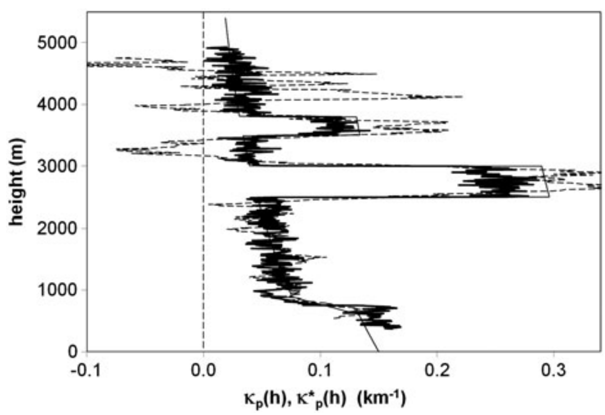

Fig. 8. Vertical profiles of the particulate extinction coefficient retrieved from the signal measured at $\varphi_i = 45°$. The thin solid curve is the model profile, the same as that in Fig. 7, and the thick solid curve is the profile derived with the new technique. The dashed curve shows the profile of $\kappa^*_p(h)$ retrieved using the derivative with the slope range resolution of 510 m.

light, a 25 cm UV enhanced Schmidt–Cassegrain telescope is used. The lidar operated at wavelengths of 1064 and 355 nm with 98 and 45 mJ energy, respectively; however, in this study, only data at the wavelength 355 nm are used.

The data shown in Figs. 9–11 were obtained on 27 August 2009 using 12 azimuthally averaged scans within the slope angular sector from 9° to 80°. For all elevation angles, the profiles $T^2_{\mathrm{tot},i}(0, r_i)$ were found and recalculated into the functions of height, $T^2_{\mathrm{tot},i}(0, h)$, using the dependence in Eq. (2). We present here only two arbitrarily selected functions $T^2_{\mathrm{tot},i}(0, h)$ measured in the significantly different elevation angles of 15° and 68° (Fig. 9). To extract the corresponding profiles of the particulate extinction coefficient, eight overlapping intervals for each slope direction were used, the same number as in our numerical experiments. To reduce the error due to the likely existence of the nonzero aerosol loading at high altitudes, the constant $C_{\max}$ found with Eq. (18) was reduced by 10%. In Figs. 10 and 11 the particulate extinction coefficients versus height, extracted from the profiles $T^2_{\mathrm{tot},15}(0, h)$ and $T^2_{\mathrm{tot},68}(0, h)$, are shown. In addition to simple averaging of $\kappa_p(h)$ in the overlapping areas, as was done in our simulations, the weighted averaging of the extinction coefficient was also performed. The weight function of the extinction coefficients over each overlapping zone (r_m, r_n) was calculated as

$$w = \left\{ \frac{1}{n(r_m, r_n)} \sum_{r_m}^{r_n} [\langle T^2_{p,i}(r_m, r_i) \rangle - T^2_{p,i}(r_m, r_i)]^2 \right\}^{-1}, \quad (21)$$

where $n(r_m, r_n)$ is the number of data points within the selected overlapping interval (r_m, r_n). In both figures, the thick gray curves are the average profiles of stepwise extinction coefficient $\kappa_p(h)$, whereas the thick black curves are the weighted averages of $\kappa_p(h)$. When there are no sharp changes in the lidar ratio within the piecewise range (r', r''), the weighted and the nonweighted averages yield close retrieval results. If such sharp changes of the lidar ratio take place, the weighted average yields a more accurate result. Accordingly, the increased discrepancy of these two averages in the experimental data shows the areas of increased changes in the lidar ratio, where the assumption of the invariable lidar ratio function $S_{p,i}(r', r_i)$ within the range (r', r'') does not properly hold.

Here some clarification of specifics in the presentation of our experimental results is required. Lidar measurements deal with a typical ill-posed problem, so that no rigid estimation of the accuracy of the retrieved profiles is possible. Meanwhile, different retrieval variants allow determining (a) what discrepancies between the extracted profiles in $\kappa_p(h)$ exist when different *a priori* assumptions are used for the retrieval, and (b) what are the heights where the different assumptions yield the small profile divergence acceptable for the researcher's measurement task. The extinction coefficient $\kappa_p^*(h)$ retrieved with the

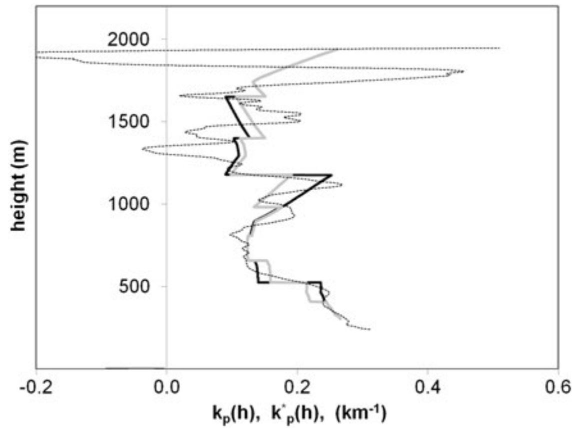

Fig. 10. Particulate extinction-coefficient profiles retrieved from $T^2_{\mathrm{tot},15}(0, h)$ calculated for the elevation angle $\varphi_i = 15°$. The thick gray curve shows the average profile of stepwise extinction coefficient $\kappa_p(h)$, and the thick black curve is the same profile obtained with the weighted average. The dashed–dotted curve is the profile $\kappa_p^*(h)$ obtained through numerical differentiation with the slope resolution of ~500 m.

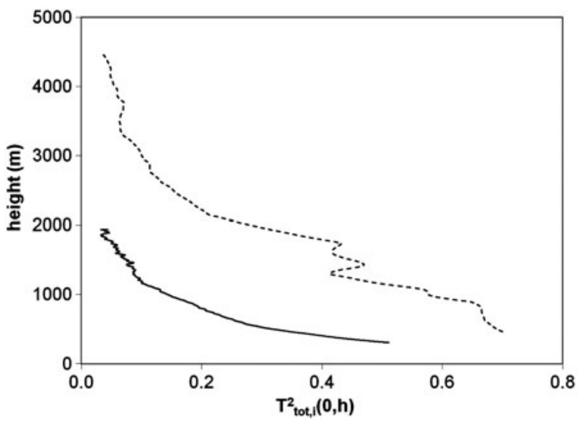

Fig. 9. Transmittance profiles $T^2_{\mathrm{tot},15}(0, h)$ (solid curve) and $T^2_{\mathrm{tot},68}(0, h)$ (dotted curve) measured from the azimuthally averaged lidar signals recorded in the elevation angles 15° and 68°.

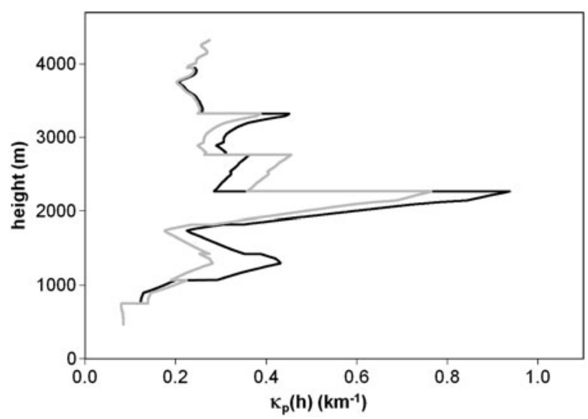

Fig. 11. Particulate extinction-coefficient profiles retrieved from $T^2_{\mathrm{tot},68}(0, h)$. The thick gray curve shows the average profile of stepwise extinction coefficient $\kappa_p(h)$, and the thick black curve is the profile obtained with the weighted average.

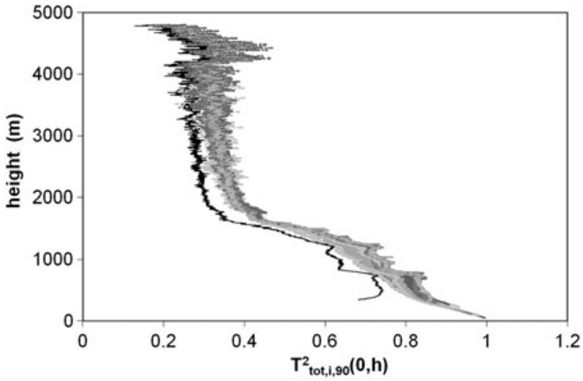

Fig. 12. Slope profiles of vertical transmittance $T^2_{\mathrm{tot},i,90}(0,h)$ obtained from azimuthally averaged signals. The black solid curve on the left is the profile retrieved for the slope direction of $\varphi_i = 80°$.

slope range resolution 500 m is also shown in Fig. 10 (the dotted curve). This profile, derived through numerical differentiation, agrees well with two others up to the height ~1200 m, and then large erroneous fluctuations take place; however, these fluctuations are centered close to two other profiles, which, in turn, are close to each other. One can conclude that the assumption of the range-independent $S_{p,i}(r', r_i)$ over the selected piecewise ranges has been met and the extracted profiles of the extinction coefficient can be trusted.

Let us consider the simplest variant that allows excluding the poor data that can distort the profile of $[C\beta_{\pi,p}(h)]$ in the Kano–Hamilton solution. In this variant, the profile of the two-way transmittance versus height is determined using the data of the whole lidar scan without determining each separate profile of $\kappa_p(h)$ in the scan. To clarify this variant, we will discuss the experimental data measured with the lidar in the clear atmosphere on 16 September 2008. As in the previous case, 12 azimuthally averaged scans were performed within the vertical sector from 9° to 80°. After determining the function $[C\beta_{\pi,p}(h)]$, the slope profiles $T^2_{\mathrm{tot},i}(0, r_i)$ for all elevation angles were found and recalculated into the functions of height $T^2_{\mathrm{tot},i}(0,h)$. Then all the functions $T^2_{\mathrm{tot},i}(0,h)$ were recalculated into the vertical transmittance profiles using the formula $T^2_{\mathrm{tot},i,90}(0,h) = [T^2_{\mathrm{tot},i}(0,h)]^{\sin\varphi_i}$. In Fig. 12, the full set of these functions is shown as the cluster of gray and dark gray curves. Aside from the profile determined in the slope direction of 80°, all other functions are close to each other. Accordingly, the function at $\varphi_i = 80°$ has to be excluded from the data processing, and the assumption in Eq. (2) is valid for the angle sector from 7.5° to 68° only. Having the set of functions $T^2_{\mathrm{tot},i,90}(0,h)$, one can determine an average function and use it to extract the extinction coefficient $\kappa_p(h)$ from the entire lidar scan rather than for the individual elevation angles. However, the bulges at individual curves may create corresponding bulges in the averaged transmittance profiles, causing significant distortion of the retrieved extinction coefficient. In our case, the use of minimal values of the profiles

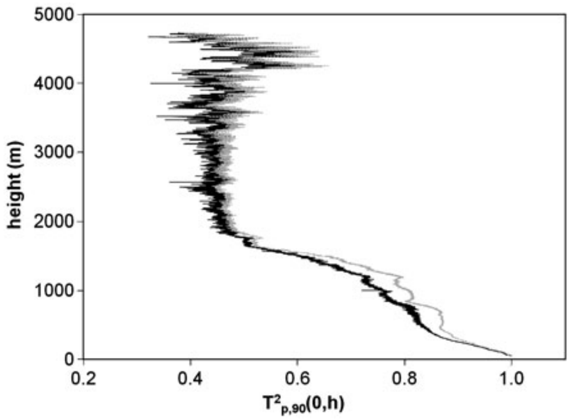

Fig. 13. Two-way particulate transmittance profiles extracted from the set of profiles shown in Fig. 12. The gray curve shows the average particulate profile $T^2_{p,\mathrm{aver},90}(0,h)$, and the black curve shows the minimal profile $T^2_{p,\min,90}(0,h)$. Both profiles are obtained after excluding $T^2_{\mathrm{tot},80}(0,r_{80})$.

$T^2_{\mathrm{tot},i,90}(0,h)$, instead the averaged profiles, results in a more smoothed function. In Fig. 13, two alternative particulate transmittance profiles are shown, extracted from the profiles in Fig. 12 after the exclusion of that at $\varphi_i = 80°$. The gray curve shows the average particulate transmission profile $T^2_{p,\mathrm{aver},90}(0,h)$ obtained from the average of $T^2_{\mathrm{tot},i,90}(0,h)$ after excluding the molecular component; the black curve shows the same vertical profile, $T^2_{p,\min,90}(0,h)$, but obtained using the minimal values of $T^2_{\mathrm{tot},i,90}(0,h)$. The profile $T^2_{p,\min,90}(0,h)$ has significantly fewer bulges and concavities over the altitude range from ~400 to 1300 m; it can be considered as an estimate of the maximal aerosol loading in the searched atmosphere.

In Fig. 14, the particulate extinction-coefficient profiles versus height are shown, obtained from $T^2_{p,\min,90}(0,h)$ in Fig. 13. As in the previous example, before determining $\beta_{\pi,p}(h)$, the constant $C_{\max}$ was decreased by 10%. Similar to Figs. 10 and 11, the thick

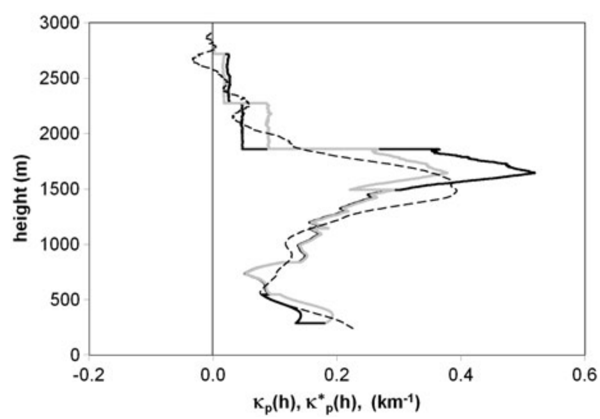

Fig. 14. Particulate extinction-coefficient profiles retrieved from $T^2_{\mathrm{part},\min,90}(0,h)$. The thick gray curve shows the average profile of stepwise extinction coefficient $\kappa_p(h)$, and the thick black curve is the same profile obtained using the weighted average. The dashed curve is the profile obtained through the numerical differentiation of the profile $T^2_{\mathrm{part},\min,90}(r_{\min}, r_i)$ using the resolution range of ~500 m.

gray curve shows the average profile of the stepwise extinction coefficient $\kappa_p(h)$, and the thick black curve is the weighted average of $\kappa_p(h)$. The dashed curve shows the profile $\kappa_p^*(h)$ extracted through numerical differentiation; here, the height resolution 500 m was used. In these results, different retrieval methods yield relatively similar results. The discrepancy in these curves slightly increases in the heterogeneous area and at the far end, where the numerical differentiation yields minor erroneous negative values of the extinction coefficient.

4. Summary

In this study, a modified data-processing technique for multiangle measurements in clear and moderately polluted atmospheres is discussed. The key subject of interest, the extinction-coefficient profile, is extracted from the backscatter term of the Kano–Hamilton solution and the lidar signal measured under the selected elevation angle. For the selected direction, the local stepwise column-integrated lidar ratios over restricted ranges are found from which the piecewise extinction coefficient is derived. Such an approach allows extracting the extinction-coefficient profile both along individual elevation angles and in the vertical direction.

The method allows one to analyze the signals measured in different slope directions and reject the signals that do not obey the condition of atmospheric homogeneity or have significant systematic distortions. Using this technique, one can determine, (i) whether the requirements in Eqs. (1) and (2) are satisfactorily met, (ii) the elevation angles in which these conditions are not valid, (iii) whether the individual signals are significantly corrupted, and (iv) how significant are the discrepancies between the profiles extracted under different elevation angles at different altitudes.

Unlike the differentiation method, the new technique enables discrimination of thin stratified layering with sharp boundaries at the far-end range. The approach used in this study also allows more realistic estimation of the distortions of the inversion results when compared to the methods based entirely on statistics, when no systematic instrumental errors are taken into consideration.

This method was used to process the experimental data obtained with the Fire Sciences Laboratory lidar both in clear-air conditions and in the vicinity of wildfires, and has demonstrated its value for future applications.

References

1. M. Kano, “On the determination of backscattering and extinction coefficient of the atmosphere by using a laser radar,” Papers Meteorol. Geophys. **19**, 121–129 (1968).
2. P. M. Hamilton, “Lidar measurement of backscatter and attenuation of atmospheric aerosol,” Atmos. Environ. **3**, 221–223 (1969).
3. V. A. Kovalev and W. E. Eichinger, *Elastic Lidar. Theory, Practice, and Analysis Methods*, (Wiley-Interscience, 2004), pp. 295–304.
4. D. N. Whiteman, “Application of statistical methods to the determination of slope in lidar data,” Appl. Opt. **38**, 3360–3369 (1999).
5. S. N. Volkov, B. V. Kaul, and D. I. Shelefontuk, “Optimal method of linear regression in laser remote sensing,” Appl. Opt. **41**, 5078–5083 (2002).
6. F. Rocadenbosch, A. Comeron, and D. Pineda, “Assessment of lidar inversion errors for homogeneous atmospheres,” Appl. Opt. **37**, 2199–2206 (1998).
7. L. Fiorani, B. Calpini, L. Jaquet, H. Van den Bergh, and E. Durieux, “Correction scheme for experimental biases in differential absorption lidar tropospheric ozone measurements based on the analysis of shot per shot data samples,” Appl. Opt. **36**, 6857–6863 (1997).
8. M. Adam, V. Kovalev, C. Wold, J. Newton, M. Pahlow, Wei M. Hao, and M. B. Parlange, “Application of the Kano-Hamilton multiangle inversion method in clear atmospheres,” J. Atmos. Ocean. Technol. **24**, 2014–2028 (2007).
9. G. J. Kunz and G. de Leeuw, “Inversion of lidar signals with the slope method,” Appl. Opt. **32**, 3249–3256 (1993).
10. V. Shcherbakov, “Regularized algorithm for Raman lidar data processing,” Appl. Opt. **46**, 4879–4889 (2007).
11. B. Cadet, V. Giraud, M. Haeffelin, P. Keckhut, A. Rechou, and S. Baldy, “Improved retrievals of the optical properties of cirrus clouds by a combination of lidar methods,” Appl. Opt. **44**, 1726–1734 (2005).
12. V. Kovalev, “Determination of slope in lidar data using a duplicate of the inverted function,” Appl. Opt. **45**, 8781–8789 (2006).
13. V. A. Kovalev, W. M. Hao, and C. Wold, “Determination of the particulate extinction-coefficient profile and the column-integrated lidar ratios using the backscatter-coefficient and optical-depth profiles,” Appl. Opt. **46**, 8627–8634 (2007).
14. V. Kovalev, C. Wold, W. M. Hao, and B. Nordgren, “Improved methodology for the retrieval of the particulate extinction coefficient and lidar ratio from the lidar multiangle measurement,” Proc. SPIE **6750**, 67501B (2007).
15. G. Pappalardo, A. Amodeo, M. Pandolfi, U. Wandinger, A. Ansmann, J. Bösenberg, V. Matthias, V. Amiridis, F. De Tomasi, M. Frioud, M. Iarioti, L. Komguem, A. Papayannis, F. Rocadenbosch, and X. Wang, “Aerosol lidar intercomparison in the framework of the EARLINET project. 3. Raman lidar algorithm for aerosol extinction, backscatter, and lidar ratio,” Appl. Opt. **43**, 5370–5385 (2004).
16. S. Godin, A. Carswell, D. Donovan, H. Claude, W. Steinbrecht, I. McDermid, T. McGee, M. Gross, H. Nakane, D. Swart, H. Bergwerff, O. Uchino, P. Gathen, and R. Neuber, “Ozone differential absorption lidar algorithm intercomparison,” Appl. Opt. **38**, 6225–6236 (1999).